Hysteretic model of steel connections for self-centering frames based on experimental studies of angles

*Arturo López-Barraza[1], Sonia E. Ruiz[2],
Alfredo Reyes-Salazar[3] and Edén Bojórquez[4]

[1], [2] *Instituto de Ingeniería, UNAM, Coyoacán, México D.F., C.P. 04510*
[3], [4] *Facultad de Ingeniería, UAS, Culiacán, Sinaloa, México, C.P. 80040*
[1] *alopezb@uas.edu.mx*

ABSTRACT

Because brittle failure is prevented and because of their self-centering connection capacity, steel frames with post-tensioned bolted connections are a viable option in high seismicity areas,. The angles have a dominant influence on the performance of the post-tensioned semi-rigid connections; therefore, it is necessary to know the capabilities in terms of stiffness, strength, ductility and energy dissipation. In this paper a set of 15 experiments with angles of 152 x 152 x 10 mm and different gage values were developed. For this aim, monotonic and cyclic tests with increasing ductility demands were performed. The results obtained are used to propose equations to calculate the initial and post-yielding stiffness. An alternative definition of ductility is proposed and fatigue curves and hysteretic energy (E_H) capacity are estimated. Additionally, it is proposed a function that reproduces the hysteretic cycles obtained experimentally with good accuracy. The results were extended for the application to post-tensioned top and seat connections, and a continuous function which defines the *M-θr* hysteretic curve is suggested. The proposed equations fit well with the experimental results found in the literature. It is concluded that the capacity of E_H decreases as the ductility demand increases, that the total hysteretic energy capacity in the steel angles is constant for different gages and that the number of cycles of load to failure decreases as the ductility demand increases.

1. INTRODUCTION

Due to the need of preventing brittle failure in welded connections of moment resisting frames (MRF), after the 1994 Northridge Earthquake, various researchers suggested replacing welded connections for semi-rigid connections (SRC) because they are more effective to prevent this type of damage. In fact, analyses of steel frames with semi-rigid connections (SRF) under earthquake ground motions have shown that the maximum values of the base shear and drifts are reduced compared with their counterparts with rigid connections; moreover, they dissipate more energy (Nader 1991, Leon 1995, Reyes-Salazar 2000). To increase the rigidity of the connections and

---

[1] Ph.D. Student
[2], [3] Professors

to reduce the residual drift Ricles (2001) proposed post-tensioning the SRF with high strength strands symmetrically positioned parallel to the axis of the beams and anchored at the ends of the frames. It was observed that the performance of this new type of structure is superior compared with the traditional MRF (Ricles 2002, Christopoulos 2002b, Garlock 2009, Chou 2010a, Chou 2011, López 2013).

The post-tensioned steel frames (PTSF) are a viable alternative to replace frames with welded connections in high seismic areas. There are two types of common devices used to dissipate energy in PTSF which depends on the relative rotation of beam-column joint (θ_r). The first consists of elements that dissipate energy by plastic deformation (hysteretic dissipators), and can be angles, plates o bars bolted to the connection (Ricles 2001, Christopoulos 2002a, Garlock 2005, Garlock 2007, Chou 2010b). The other devices are usually plates placed on the flange or the web of the beam and connected to the column which dissipates energy by friction (Rojas 2005, Wolski 2009, Guo 2011). They have numerous advantages of PTSF such as: preventing brittle fracture of the connection, field welding is not required, the connection is made with conventional materials and skills, and the damage is concentrated in the dissipater elements maintaining essentially elastic beams and columns after strong earthquakes. The connection has a initial stiffness similar to that of a typical welded connection, and it is self-centering without residual deformation. In some studies of this type of structural system it has been found that drifts and residual drifts decrease, avoiding higher costs of repairing or permanent loss of functionality of the building after a strong earthquake (McCormick 2008, López-Barraza 2013). If required, it is economical and easy to replace the damaged angles, shortening the time of interference in the use of the building.

The rigorous analysis of the PTSF is more complex than that of frames with rigid or pinned connections. It is difficult to capture the behavior of the bolted connections due to their large number of components that have a large influence on the performance. These components are: angles or bolted plates; the presence or absence of reinforcing plates; the size, strength, torque and position (gage) of the screws. Additionally, it is necessary to determine the influence and contribution of post-tensioned elements.

PTSF connections are basically SRC with post-tensioned (PT) elements which can be idealized as two springs in parallel, one nonlinear and one linear, representing the SRC and the PT elements, respectively.

The presence of the SRC has been studied mainly in two ways; the first considers the connection as a single piece, and describes its behavior using the moment- rotation curve (M-θ_r) (Richard 1975, Yang 2009). The parameters of the corresponding equations are usually obtained from experimental results. In the second option the parts of the connection are modeled with finite elements using fiber elements, assigning to each fiber a force-displacement relationship (Shen 2000, Ricles 2001). The first option has the advantage that when implemented it in a frame analysis program the number of elements required is reduced. However, the disadvantage is that no information is provided on the performance of the parts of the connection.

With the purpose of determining the performance and evaluating the influence of the elements that compose the semi-rigid post-tensioned connection, experiments have been developed finding that the behavior is nonlinear from the start of the deformation (Ricles 2001, Ricles 2002, Garlock 2005, Chou 2010b). The typical M-θ_r curve is

shaped flag, which characterizes the capacity of self-centering and energy dissipation. In these studies, the proposed hysteretic models have been fitted with straight segments (bi-linear or multi-linear). In the case of connections with bolted angles, it is very important to know the performance of the angles because its influence on the behavior of the connection. With the aim of determining their initial and post-yielding stiffness, strength, ductility, low cycle fatigue and hysteretic energy dissipation capacity, experiments have been conducted with isolated angles of 8, 10, 13, 16 and 19 mm thick (Shen 1999, Garlock 2003) by changing the gage, size and strength of screws and the type of load. It has been found that the ultimate strength is 3 times the yield strength, that the hysteresis loops are stable that degradation of strength and stiffness don't occur, and that the ductility capacity ranges between 8 and 10.

This study aims to improve the understanding of the performance of connections with bolted top and seat angles, post-tensioned with high strength strands. In order to observe the performance of the angles used in the connections, the authors developed a series of 15 experiments with angles of 152x152x10 mm for different gage values, subjected to cyclic loading, increasing the ductility demands. From the results, equations to calculate initial and post-yield stiffness are proposed. A new definition of ductility is suggested, fatigue and hysteretic energy capacity curves are built as a function of ductility demand. Additionally, it is proposed a continuous function that accurately reproduces the hysteretic cycles obtained experimentally. The results obtained for isolated angles, were extended for the application to the post-tensioned top and seat connection and a continuous function which defines the M-θ_r curve of the hysteretic cycles is proposed. The proposed equation satisfactorily fits the experimental results found in the literature.

2. EXPERIMENTAL PROGRAM

2.1 Test specimen and instrumentation

The general configuration of the test specimens is shown in Fig.1a, to achieve symmetry, each specimen consists of two angles placed back to back, A490 steel screw with diameter of 25.4 mm are used to attach the angles to the loading machine. The mechanical properties, obtained from the average of 2 coupons are: yield stress (Fy) = 382 MPa, ultimate strength (Fu) = 552 MPa, modulus of elasticity (E) = 213 GPa and yield strain (ξ_y) = 0.002. A load of magnitude 2V is applied with an actuator as shown in Fig. 1 (a), by symmetry each angle support a load of magnitude V. The displacement of the heel angle with respect to the column flange (Δ) is measured using a LVDT of 25 mm (see Fig. 1 c). To measure displacements at various points of interest a camera KRYPTON K600 was used, Fig. 1 (a) shows the location of ten LED sensors. Based on their relative displacements the following can be measured:
- L3 and L6 measure Δ (check the LVDT displacements)
- L4 and L7 measure axial strain of the bolts.
- L1 and L3, L3 and L5 measure the axial deformation of the angle wings.
- L1 and L2, L5 and L6, measure the relative angle sliding with respect to the beam and column flanges respectively.

- L6 and L8 measure the deformation of the simulated column.
- L8 and L9 measure the axial strain of the bolt.
- L9 and L10 measure the displacement of the actuator piston (check the displacements of the internal meter of the MTS).
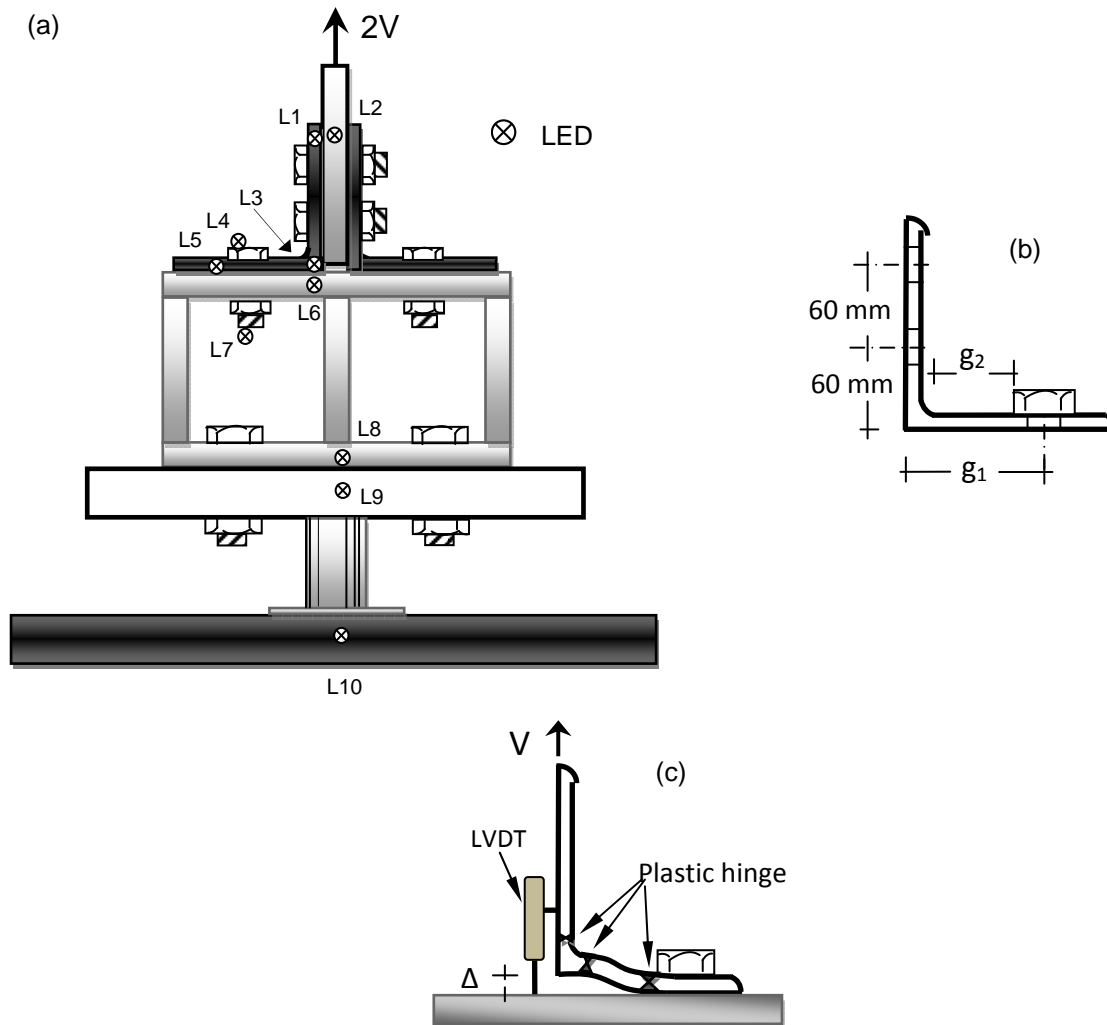

Fig. 1 Experimental model

2.2 Ductility definitions

Ductility (μ) is usually defined as the ratio of Δ_{max} to Δ_y. There are several alternatives to define the yield displacement at the angles. Δ_y may be regarded as the displacement when the first fiber yield, or that produced when the angle mechanism occurs. Such deformation states correspond to the beginning and the end of the transition zone respectively in the V-Δ graph, bounded by Points 1 and 2 shown in Fig. 2. Shen (1999) assume that Δ_y corresponds to the plastic mechanism formation from which ductility values from 8 to 10 are reported. Since for the first load levels, the

stresses in the angles are due to bending and shear, yielding of the material gradually occurs with different intensity in each section, therefore, it is not observed a sudden loss of rigidity, but it occurs in a wide range of displacements already defined as the transition zone. Considering that the capacity to dissipate E_H of the angles is an important parameter, a value of Δ_y obtained from the intersection of two straight lines as shown in Fig. 2 is suggested in this study, in such a way that the enclosed areas by these lines and the V-Δ monotonic are the same. Table 2 shows the values of Δ_y obtained according to this definition.
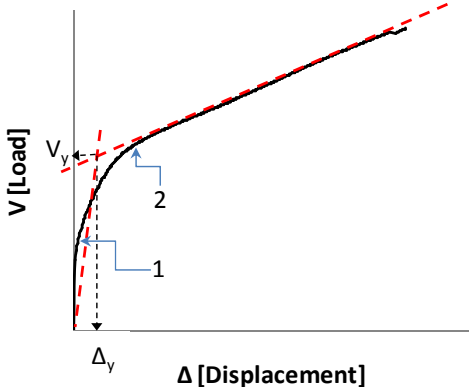

Fig. 2 transition zone on the monotonic curve

2.3 Test sequence

Monotonic and cyclic tests for a total of 15 specimens were developed, with gage (g_1) of 80, 90, 100 and 108 mm. For each g_1, a test was carried out monotonically from which the yield displacement (Δ_y), the yield strength (V_y), the maximum displacement (Δ_{max}) and the maximum force (V_{max}) were determined, as defined below.

After obtaining Δ_y, cyclic tests were performed for each gage with maximum ductility demands of 3, 6, 12 and 18. Table 1 shows the pattern of cyclic loading controlled by

Table 1 Loading History

Load step	No. Of cycles	Cycle number	Δ
1	6	1 - 6	$0.3\Delta_y$
2	6	7-12	$0.6\Delta_y$
3	4	13-16	$1.0\Delta_y$
4	2	17-18	$1.5\Delta_y$
5	2	19-20	$2.0\Delta_y$
6	2[a]	21-22 (21→)	$3.0\Delta_y$
7	2[a]	23-24 (23→)	$6.0\Delta_y$
8	2	25-26	$9.0\Delta_y$
9	2[a]	27-29 (27→)	$12.0\Delta_y$
10	…[a]	30→	$18.0\Delta_y$

[a] Cycle was repeated until the specimen failed

displacements, which is similar to that proposed by the SAC (SAC/BD 1997). The amplitudes in each cycle are modified in proportion to Δ_y, until the Δ_{max} corresponding to the ductility demand imposed on each test is reached. For the ductility of 3, 6, 12 and 18 the loading and reloading process is maintained until failure occurs. The loading speed in all cases was 1.5 mm/s.

Table 2 shows the specimens tested for some experimental results. The parameter used in the specimen names are self-explaining, for example L152-10-g90-D6 means that a sided angle of 152 mm, 10 mm thick, 90 mm gage and a ductility demand of 6, were considered. The letter M in the Table 2 corresponds to a monotonic test. Fig. 1 (b) shows the gage (g_1) and the effective gage (g_2), the first is defined as the distance from angle heel to the screw center, and the second as the distance from the fillet side angle to the screw head, which is precisely the point where plastic hinges are formed. g2 largely defines the stiffness and the ductility and depends on the thickness of the angle, the size of the screws, and g1.

Table 2 Test specimens

No	Name	g_2/t	Δ_y (mm)	Δ_m (mm)	μ	V_y (kN)	V_m (kN)	K_{ei} (kN/mm)	K_p (kN/mm)	Cycles	E_H (kN.m)
1	L152-10-g80-M	3.9	0.60	12.7	*	65.0	110.4	45.79	6.67	*	*
2	L152-10-g80-D12	3.9	*	7.2	12	*	95.2	68.15	*	118	33.05
3	L152-10-g80-D18	3.9	*	11.0	18	*	103.7	140.40	*	61	23.60
4	L152-10-g90-M	5.0	1.00	19.8	*	50.0	103.2	24.66	3.10	*	*
5	L152-10-g90-D3	5.0	*	3.0	3	*	57.0	57.56	*	1559	51.00
6	L152-10-g90-D6	5.0	*	6.0	6	*	73.0	77.44	*	213	42.50
7	L152-10-g90-D12	5.0	*	12.0	12	*	88.6	76.61	*	43	24.65
8	L152-10-g90-D18	5.0	*	18.0	18	*	99.3	60.25	*	25	17.35
9	L152-10-g100-M	6.0	1.70	18.0	*	47.5	87.7	26.40	2.32	*	*
10	L152-10-g100-D3	6.0	*	5.1	3	*	74.8	49.43	*	359	48.10
11	L152-10-g100-D6	6.0	*	10.2	6	*	67.9	28.91	*	116	42.25
12	L152-10-g100-D11	6.0	*	18.0	11	*	89.0	29.11	*	43	29.55
13	L152-10-g108-M	6.9	1.75	22.0	*	40.0	78.1	14.41	2.00	*	*
14	L152-10-g108-D6	6.9	*	10.5	6	*	64.8	29.67	*	90	33.90
15	L152-10-g108-D10	6.9	*	18.0	10	*	78.1	20.75	*	32	29.70

3. EXPERIMENTAL RESULTS

3.1 Failure patterns

Fatigue failure occurred in the angles in all cases. Because of the large size and strength of the bolts, they remained perfectly elastic. A mechanism with three plastic hinges was formed; the first parallel to the face of the column screws and the others in the angle fillets, (see Fig. 1c). Fractures occurred in the fillet angle on the side of the column, excepting for the Specimens 5 and 10; in these cases the screws are loosened

losing clamping with the column, allowing greater freedom of rotation and the fracture at the fillet on the side of the beam. In the monotonic tests, Δ corresponding to the first flow is almost unnoticeable. When the mechanism is formed, Δ values were observed to be 2.3, 3.3, 4.5 and 5.5 mm in the specimens, for gages of 80, 90, 100 and 108 mm, respectively. From the displacements recorded by the LEDs, it is observed that the bolts remain elastic, axial strains in the wings of the angles are negligible compared to Δ. There was no sliding of the angles relative to the beam. In the Specimens 5 to 10 small displacements relative to the column flange were observed since, as already mentioned, due to the number of cycles the bolts lost some tightening. In spite of this no significant influence was observed in the hysteresis loops.

3.2 Stiffness

The initial stiffness (K_{ei}) corresponds to the elastic behavior, it was determined by averaging the rigidity obtained in the first cycles of loading in the range of very small deformations before the transition. All of these cycles start at 0.05 mm and finalize between 0.2 and 0.6 mm, according to the gage increment. The post-yielding stiffness (K_p) is calculated after the transition zone, this remains practically constant until the maximum displacement of the cycle. Table 2 shows the values of K_{ei} and k_p. The reason of K_p to K_{ei} (r_p) varies from 0.09 to 0.15. Fig. 3 shows the results of Specimens 9 and 12, which correspond to a monotonic and a cyclic test with the same gage respectively, and the same ductility demand. It can be observed that:

- The monotonic test curve is the envelope of the hysteretic cycles.
- The origen of the reloading curve changes when increasing the cycle amplitude, however, it always cross the end point of the previous cycle. It indicates a hysteretic cycle shift which is produced by the Bauschinger effect.
- There is no appreciable loss of initial stiffness.
- There is an increment of K_p for the cycles with large displacements due to strain and geometry hardening (Shen 1999, Garlock 2003).
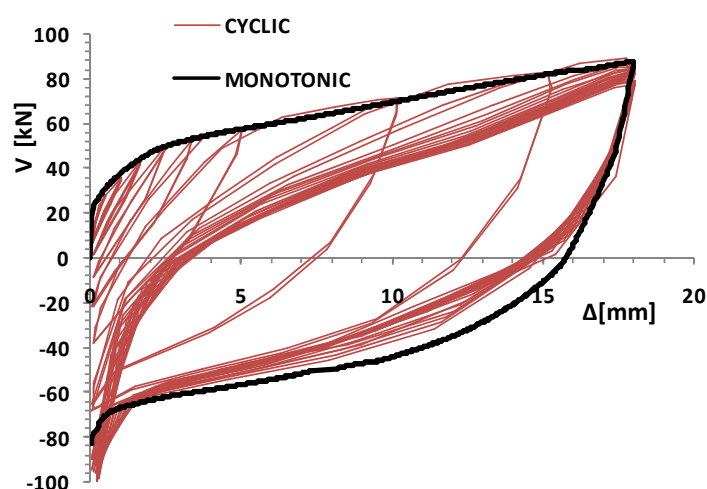

Fig. 3 Monotonic and cyclic tests (specimen 9 and 12)

3.3 Number of load cycles

Some zones of the world are exposed to strong earthquakes of large duration, as those occurred in Mexico City in 1985, in Chile in 2010 and in Japan in 2011. This implies that the structures are subjected to a large number of loading and unloading cycles and changes in the direction of the stresses in structural elements and connections. Table 2 shows the number of cycles to failure of the tested angles; it is clear that the capacity of number of cycles decreases rapidly as µ increases. Fig. 4 shows the number of cycles (CN) obtained from the experiments for each µ, the distribution of the results become asymptotic to the axes, that is, the number of cycles tends to zero as the ductility demand tends to infinity. By using regression analysis of the experimental results Eq. (1) is obtained. With this equation the maximum number of cycles that the angle supports can be calculated for a specified ductility demand. Eq. (1) is plotted in Fig. 4 and is known as the fatigue curve.
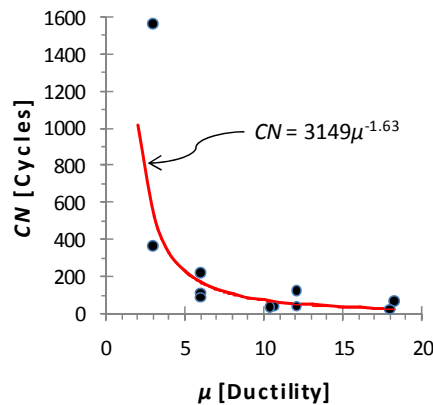
$$CN = 3149\mu^{-1.63} \tag{1}$$

Fig. 4 Fatigue curve

3.4 Hysteretic energy

In the case of PTSF with top and seat connection, the angles are the main elements that dissipate E_H. It is important to know the significant variables that affect its energy dissipation capacity. E_H is the sum of the areas enclosed in the hysteresis cycles up to failure. It is known to be a direct function of the volume of material that yields, then, E_H increases when the size of the angle increases, and grows faster with increasing the angle thickness (Shen 1999, Garlock 2003). Fig. 5 shows graphs of E_H vs. μ for each gage obtained from Table 2, it can be observed that:

- For a given μ, E_H does not vary with g_2.
- For a given g_2, E_H decreases as μ increases.
- In all cases, when µ decreases E_H increases. The reason for this, is that, although the cycle amplitudes are small, the number of cycles to failure

increases.

- There is a linear variation between E_H and μ.

By regression analysis of the experimental results Eq. (2), to calculate the E_H as a function of μ, is obtained. It is only valid for steel G50 angles of 152 x 152 x 10 mm and 152 mm length.

$$E_H = 51.84 - 1.849\mu \text{ kN.m} \tag{2}$$

The hysteretic energy dissipated per unit length of the angles (E_{Hb}) can be calculated as follows

$$E_{Hb} = \frac{E_H}{b} \tag{3}$$

where b is the length of the angle. By taking b=152 mm and applying Eq. (3) to the results of this study, Eq. (4) is obtained, which is valid to calculate the hysteretic energy capacity per unit length, for angles of 10 mm thickness and any gage amplitude.

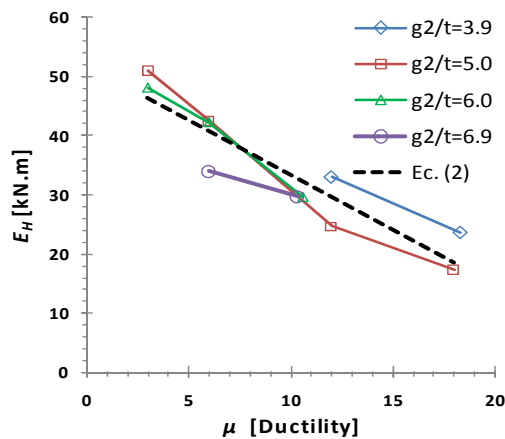$$E_{Hb} = 0.341 - 0.012\mu \text{ kN. m/mm} \tag{4}$$

Fig. 5 Hysteretic energy capacity of angles

4. ANALYTICAL MODEL FOR INITIAL STIFFNESS

To estimate the initial stiffness, the angle is idealized as a structure frame and then the displacement method (Weaver 1980) is used to find the relationship between force and displacement in the elastic range. Fig. 6 shows the model used; without considering axial deformation it has two degrees of freedom in the node B: a linear displacement in y direction (δ) and the angular displacement (θ). The node A is fixed and represents the action of the column screw, the node C is restricted in the x direction and to the rotation; but it is free in the y direction. The rigidity EI is constant for the portions AB and BC of the idealized angle. The lengths g_c and g_v are parallel to the

column and beam axis, respectively. The force V is applied to the end C of the member BC.
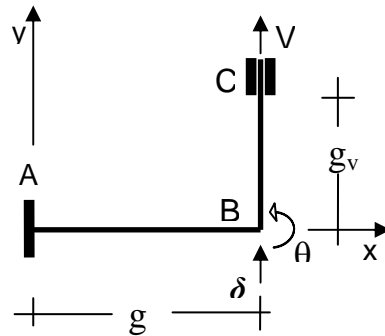

Fig. 6 Idealized angle

The details of the analysis procedure are not shown because of lack of space. It can be shown that the displacements δ and θ can be calculated as

$$\delta = \frac{g_c^3}{3EI} \frac{\left(1 + \dfrac{g_c}{g_v}\right)}{\left(1 + \dfrac{4g_c}{g_v}\right)} V \tag{5}$$

$$\theta = \frac{g_c}{2EI} \frac{1}{\left(1 + \dfrac{4g_c}{g_v}\right)} V \tag{6}$$

where, E is the elasticity modulus and I is the moment of inertia of the longitudinal section of the angle. The moments at the ends of the bars are considered positive anticlockwise and are given by Eqs. (7), (8) and (9). It must be noted that the moment M_{AB} hás the largest magnitude followed by M_{BA}, so that first plastic hinge will be formed at point A and then two plastic hinges will be simultaneously developed at point B, one at each side of the angle heel, as observed in the experiments.

$$M_{AB} = -\frac{Vg_v\left(1 + \dfrac{2g_c}{g_v}\right)}{\left(\dfrac{g_v}{g_c} + 4\right)} \tag{7}$$

$$M_{BC} = -M_{BA} = \frac{2Vg_v}{\left(\dfrac{g_v}{g_c} + 4\right)} \tag{8}$$

$$M_{CB} = \frac{Vg_v}{\left(\dfrac{g_v}{g_c} + 4 \right)}$$

(9)

Eq. (5) can be expressed as $V = K_i\Delta$ which relates the force and displacement of the angle. In this relationship

$$K_i = \frac{3EI}{g_c^3} \frac{\left(1 + \dfrac{4g_c}{g_v} \right)}{\left(1 + \dfrac{g_c}{g_v} \right)}$$

(10)

is the initial stiffness.

To calculate K_i from Eq. (10), g_c and g_v lengths are measured from the face of the screw to the outside of the angle, it gives the best approximation of the experimentally measured stiffness (K_{exp}). K_{exp} is calculated as the average of K_{ei} values for each group with the same gage by using the experimental results shown in Table 2. In general Eq. (10) overestimates the initial stiffness by about 8.5%. In Fig. 7 the ratio (CK) of K_{exp} and K_i is plotted against g_c/t. By a regression analysis the Eq. (11) is obtained, from which one can calculate the correction factor CK. Multiplying K_i per CK the corrected initial stiffness (K_i*) is obtained, which is closer to the experimental values, the average error is reduced to 2%. Table 3 shows the values of CK calculated with Eq. (11) together with Ki and $Ki*$, the last column shows the error of K_i* with respect to K_{exp}. Eq. (10) and Eq. (11) constitute a simple option to calculate the initial stiffness of such angles. There is a linear variation of the initial stiffness with respect to g_c/t, this is shown in Fig. 8 where the values of K_{exp} vs. g_c/t are plotted.

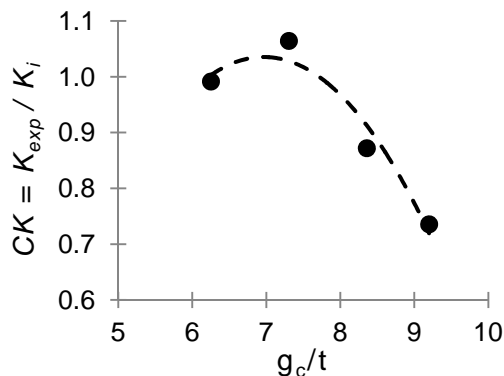$$CK = -0.063(\frac{g_c}{t})^2 + 0.882(\frac{g_c}{t}) - 2.036$$

(11)

Fig. 7 Correction factor of K_i

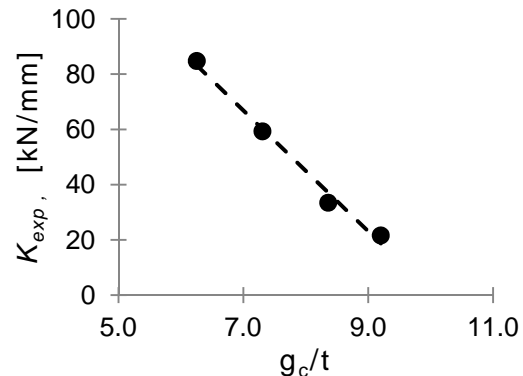Fig. 8 Variation of initial stiffness

1329

Table 3 Initial Stiffness

Specimens	g_c/t	CK	K_{exp} (kN/mm)	K_i (kN/mm)	$K_i{}^*$ (kN/mm)	% Error
1_3	6.25	1.016	84.78	85.51	86.86	2.4
4_8	7.31	1.045	59.30	55.72	58.23	-1.8
9_12	8.36	0.935	33.46	38.37	35.87	6.7
13-15	9.20	0.746	21.61	29.37	21.91	1.4

5. ANALYTICAL MODEL FOR HYSTERETIC CYCLES OF ANGLES

The dynamic analyses that reflect the actual behavior of steel frames with top and seat connections is very important to establish a mathematical model to properly reproduce the hysteretic behavior of the connection angles. Based on experimental results, some models have been proposed to represent the hysteretic cycles; Shen (2000) proposed a multi-linear model to capture the changes that occur when inelastic displacements are increased, Garlock (2003) proposed an envelope bi-linear model of the hysteretic cycles, Chou (2011) proposed a bi-linear model too using plates instead of angles. From the experimental results it was observed that the hysteresis loops are stable and remain constant for a constant ductility demand, and that there is a wide transition zone between the first yield and the formation of the mechanism (curved portion of the graph V-Δ), which makes it difficult to approximate with linear functions. To avoid this problem, in this paper an exponential equation is proposed based on the Richard Model (Richard 1975). With this continuous function, the loading and unloading cycles of the angles are modeled. This model is given by Eq. (12).

$$V = V_a - \frac{k(1-r_p)(\Delta_a - \Delta)}{\left[1 + \left|\frac{k(1-r_p)(\Delta_a - \Delta)}{\varphi V_y}\right|^N\right]^{\frac{1}{N}}} - r_p k(\Delta_a - \Delta) \tag{12}$$

Where, V = force, Δ =displacement, r_p = ratio of the initial stiffness and rigidity of post-yielding, V_y =yield force, N parameter that defines the curvature of the transition zone, φ = define the path of the unloading and reloading cycles, V_a and Δ_a are the force and displacement where the cycle starts loading or unloading. k will represent the stiffness at initial loading, which can take k_{ei} or k_i.

For additional explanation some hysteretic cycles with different ductility demands, were separated from Fig. 3, which are shown with continuous line in Fig. 9; the plot of Eq. (12) is shown with dashed line. The values of the parameters used in the equation are: k = 35.9 kN/mm (calculated using Eq. (10) and (11)), r_p=0.09, $V_y = kD_y$ = 61.0 kN, N = 1.5 and φ = 2.0. Fig. 9 shows a good approximation between hysteretic cycles obtained experimentally and those obtained from Eq. (12).

As earlier mentioned, for identical specimens, monotonic curves are the envelope of the hysteretic cycles. The monotonic curve can be adjusted with Eq. (12) by slightly

changing the values of the parameters: for the first loading (virgin curve) $\varphi = 1.0$, $\Delta_a = 0$ and $V_a = 0$. For unloading, $\varphi = 2.5$, Δ_a and V_a are the maximum values achieved in the loading cycle. k, r_p, N and V_y are unchanged. Fig. 10 shows with continuous line the monotonic curve obtained experimentally for the Specimen 9 (part of Fig. 3); the dashed line is the plot of Eq. (12).
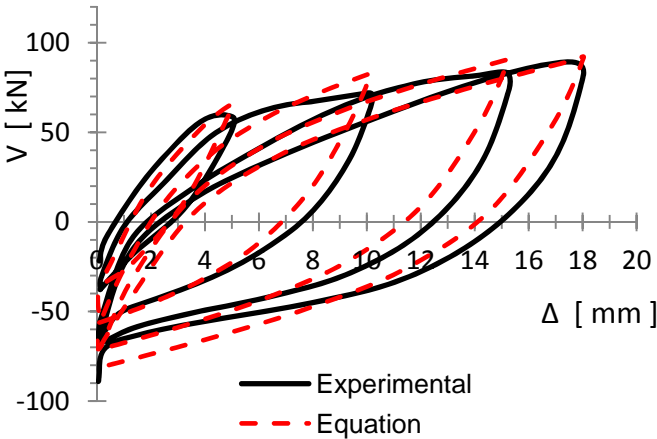
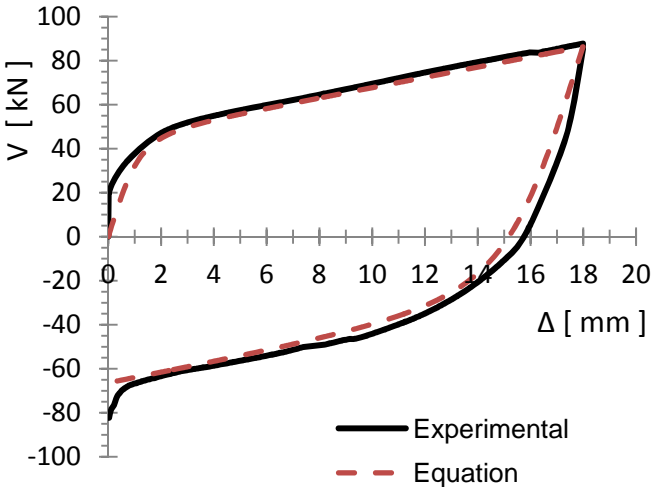Fig. 9 Hysteretic cycles of specimen L152-10-g100-D11

Fig. 10 Monotonic curve of specimen L152-10-g100-M

6. HYSTERETIC MODEL FOR POSTTENSIONED CONNECTION

6.1 Structural model of the connection

One common way of representing the hysteretic behavior of a connection is through the moment-rotation curve (M-θ_r). Figs. 11(a) and (b) show a typical assembly of a post-tensioned connection and how it is deformed by bending. θ_r is the relative rotation

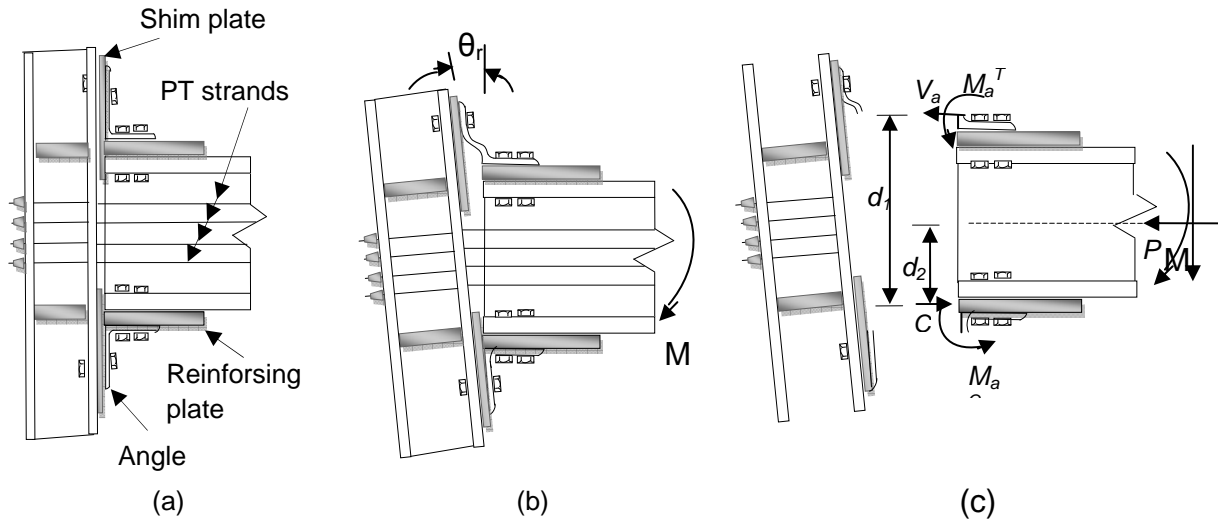of the beam axis with respect to the column and *M* is the bending moment at the end of the beam.

Fig. 11 Post-tensioned semi-rigid connection

Forces and moments acting on the connection are presented in Fig. 11(c); V_a is identified as the force in the angle and can be calculated using Eq. (12), M_a^T and M_a^C are the moments at the angles under tension and compression respectively, *P* is the resultant axial force on the beam (axial strength PT strands system is included), and C is the resultant of compression acting on the center of rotation. According to experimental studies (Garlock 2007), the rotation center is located at half thickness of the reinforcement plate of compression flange. The distances d_1 and d_2 are the lever arms measured from the center of rotation to the line of action of the forces V_a and *P* respectively.

The resultant axial force at the beam is given by

$$P = T_s + F \tag{13}$$

where T_s is the resultant of tendon force and *F* is the force induced by the interaction of the floor system with the beam. By making moment summation about the center of rotation, without considering *F*, it is obtained

$$M = T_s d_2 + V_a d_1 + M_a^T + M_a^C \tag{14}$$

Eq. (14) shows that angles and tendons work as springs in parallel, the $T_S d_2$ term represents the contribution of the post-tensioned tendon to the moment of the connection, the remaining terms are the contributions of angles. In summary, it can be stated that the flexural strength of the connection is the superposition of the contribution of the tendons and that of the angles.

6.2 Contribution of post-tensioned tendons

To obtain the M-θ_r curve of the post-tensioned tendons, it is necessary to transform the axial stiffness (k_s) of the tendons into a rotational equivalent stiffness ($k_{s\theta}$), which can be done as follows:

The tension in the tendons (T_s) is the sum of the initial tension imposed (T_0) and the additional tension caused by the connection gap (T_Δ). Thus,

$$T_s = T_0 + T_\Delta \tag{15}$$

By expressing T_Δ in terms of the connection gap (tension elongation)

$$T_s = T_0 + k_s \Delta_s \tag{16}$$

where Δ_s is the elongation of the tendons due to the gap. From in Fig. 11c, d_2 is the level arm of the resultant axial force in the beam with respect to center of rotation. Then the following relationship can be established:

$$\Delta_s = 2d_2\theta_r \tag{17}$$

The factor 2 in Eq. (17) is to consider the two connections which influence the deformation of the tendons in the interior of a bay. Substituting Eq. (17) into Eq. (16) it gives

$$T_s = T_0 + 2k_s d_2\theta_r \tag{18}$$

Eq. (18) is the relationship between the strength of the tendons and the rotation of the connection. Multiplying both sides of Eq. (18) per d_2 it is obtained

$$M_s = T_0 d_2 + 2k_s d_2^2 \theta_r \tag{19}$$

By considering

$$k_{s\theta} = 2k_s d_2^2 \tag{20}$$

and

$$M_d = T_0 d_2 \tag{21}$$

Eq. (19) can be written as

$$M_s = M_d + k_{s\theta}\theta_r \tag{22}$$

$k_{s\theta}$ in Eq. (22) is the contribution of the tendons to the rotational stiffness of the connection and M_d is known as the decompression moment. The later is the result of the initial tension so it is a constant, moreover, it represents the value of the moment just when the connection starts opening.

6.3 Contribution of the angles

The contribution of the angles to the connection resistant moment can be calculated as follow

$$M_V = V_a d_1 \tag{23}$$

In the elastic range, $V_a = K_i \Delta$, where K_i is the initial stiffness and Δ of the gap in the connection. It can established that $\Delta = d_1 \theta_r$, then $V_a = K_i d_1 \theta_r$. Substituting Eq. (23) it is obtained

$$M_V = K_i d_1^2 \theta_r \tag{24}$$

From Eq. (24) it is observed that the contribution of the angles to the rotational stiffness of the connection is

$$k_{V\theta} = K_i d_1^2 \tag{25}$$

6.4 Combined model for tendons and angles

Since only the angles exhibit nonlinear behavior, the shape of the hysteretic cycle of a post-tensioned connection is similar to that previously defined in Eq. (12). Based on this equation, and adding the contribution of tendons, Eq. (26) can be written, which defines the M-θ_r curve, for the hysteretic cycles of the post-tensioned semi-rigid connection.

$$M = M_a - \frac{k_{V\theta}(1-r_p)(\theta_a - \theta_r)}{\left[1 + \left| \dfrac{k_{V\theta}(1-r_p)(\theta_a - \theta_r)}{\varphi M_y} \right|^N \right]^{\frac{1}{N}}} - (r_p k_{V\theta} + k_{s\theta})(\theta_a - \theta_r) \tag{26}$$

M_a and θ_a are the moment and rotation at the beginning of each cycle of loading or unloading, for the initial loading cycle $M_a = M_d$ and $\theta_a = 0.0$, for the unloading phase M_a and θ_a takes the maximum preceding values, $M_y = V_y d_1$. r_p, N and φ have the same meaning as defined before.

To illustrate the use of Eq. (26), a connection was designed, similar angles to that of Specimen 12, were considered. The beam section is a W18 x 46 with plates 25 mm thick placed in the flanges as reinforcement. Four tendons of 150 mm^2, resistance of 279 kN and 8 m in length are used. The values of T_0, d_2, d_1, M_d, $k_{s\theta}$, $k_{V\theta}$, r_p and M_y, are 433.8, kN, 242 mm, 519 mm, 105 kN-m, 1757.8 kN-m/rad, 10235 kN-m/rad, 0.06, and 23.2 kN-m, respectively. Substituting these values in Eq. (25) with $M_a = M_d = 105$ kN.m, $\theta_a = 0$ and $\varphi = 1$ for the loading cycle, and $M_a = 222$ kN.m, $\theta_a = 0.033$ rad and $\varphi = 2$ for the unloading cycle the graph shown in Fig. 12 is obtained, which resembles the typical form of flag found in experimental studies (Ricles 2002, Garlock 2005).

6.5 Comparison with experimental results

For the purpose of validating the accuracy of Eq. (26), it is plotted and compared with experimental results of post-tensioned beam-column assemblies (semi-rigid post-

tensioned connection) developed by Garlock et al. (Garlock 2005). The specimens considered are: Spec. 16s-45, Spec. 20s-18 and Spec. 36s-30, tested under cyclic loading for different levels of drift. The specimens correspond to an interior connection. The sections of the beam and the column are W36 x 150 and W14 x 398, respectively. Angles 203 x 203 x 19 mm of 406 mm long, and plates of 25 x 356 mm with variable length are placed as reinforcement in the flanges, both of steel F_y = 345 MPa. The tendons are of 140 mm^2, steel A-416 and their number is variable. In the specimens notation "16s-18", "16s" refers to sixteen strands and "18" to the initial tension of each strand in kips.

Based on the geometry and material information reported, the required parameters in Eq. (26) are calculated. Fig. 13 reported by Garlock (Garlock 2005) shows the experimental results, the graphics obtained with Eq. (26) for specimens Spec. 16s-18, Spec. 20s-18 and Spec. 30s-36 are also presented in the Figure. The figure indicates a very good approximation between the equation plot and the experimental results that represent different combinations of relative contribution of angles and tendons, to the strength and stiffness of postensioned semi-rigid connections. The implementation of this model in a computer program for the dynamic analysis of post-tensioned frames with semi-rigid connections is simple and efficient since it is sufficient to consider the
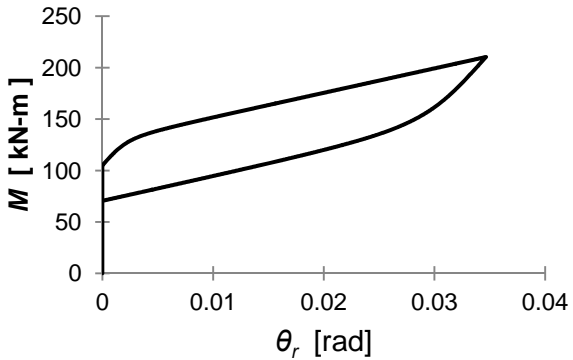

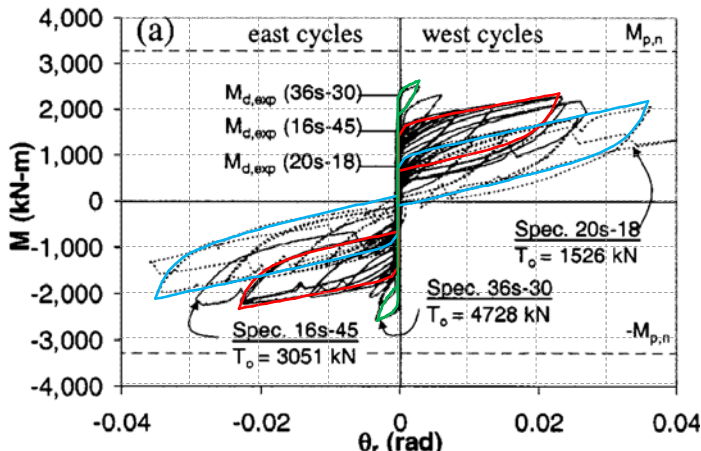Fig. 12 Typical curve $M\text{-}\theta_r$ post-tensioned semi-rigid connection

Fig. 13 Experimental results Garlock (2005) and analytical model

connection as an additional element of the structure while retaining the parameters that influence the strength, stiffness and energy dissipation capacity. An alternative very useful and powerful tool for calculating the parameters associated to the contribution of the angles in the proposed hysteretic model is the use PRCONN program developed by Richard and his associates (Richard 1993).

7. CONCLUSIONS

To improve the knowledge of the performance of steel angles used in bolted connections under cyclic loading, a set of experiments with isolates angles with different gages (g_2) was developed, in order to know the rigidity, capacity to dissipate hysteretic energy (E_H) and number of load cycles to failure for different ductility demands (μ). Mathematical models (Eq. 12) were built to represent the connections and the force-displacement hysteretic cycles (V-Δ). The results of the isolates angles were extended to post-tensioned semi-rigid connection and a continuous function (26) that accurately models the moment-rotation (M-θr) hysteretic cycles was proposed. Some important observations are:

- For a given μ, E_H does not vary with g_2.
- For a given g_2, E_H decreases as μ increases.
- In all cases, when μ decreases E_H increases.
- There is a linear variation between E_H and μ.
- There is a large variation while obtaining k_i in the experimental results, but its influence is small when compared with the large inelastic deformations, therefore, it does not significantly affect the final E_H capacity.
- The post-yielding stiffness in the angles varies from 0.09 to 0.15 of k_i.
- Hysteretic cycles are stable and no significant degradation in strength and stiffness occurs.
- Eq. (12) models with good accuracy the hysteretic cycles (V-Δ) of angles.
- Eq. (26) reproduces with good accuracy the hysteretic cycles (M-θr) of post-tensioned semi-rigid connections, so it is a good option to implement it as a hysteretic model in computer programs of nonlinear dynamic analysis.

REFERENCES

Chou, C.C. and Chen, J.H. (2010), "Column restraint in post-tensioned self-centering moment frames", *Earthq. Eng. Struct. Dyn.,* **39**(7), 751-774.
Chou, C.C. and Chen, J.H. (2010), "Tests and analyses of a full-scale post-tensioned RCS frame subassembly", *J. Construct. Steel Res.*, **66**(11), 1354-1365.

Chou, C.C. and Chen, J.H. (2011), "Analytical model validation and influence of column bases for seismic responses of steel post-tensioned self-centering MRF system", *Eng. Struct.*, **33**, 2628-2643.

Chou, C.C. and Chen, J.H. (2011), "Seismic design and shake table test of a steel post-tensioned self-centering moment frame with a slab accommodating frame expansion", *Earthq. Eng. Struct. Dyn.*, **40**, 1241-1261.

Christopoulos, C., Filiatrault, A. and Uang, C.M. (2002a), "Self-centering post-tensioned energy dissipating (PTED) steel frames for seismic regions", *University of California*, Report No. SSRP-2002/06.

Christopoulos, C. and Filiatrault, A. (2002b), "Seismic response of post-tensioned energy dissipating moment resisting steel frames", *Proceedings of the 12th European Conference on Earthquake Engineering*, London, UK, Paper No. 61.

Garlock, M., Ricles, J. and Sause, R. (2003).Cyclic load tests and analysis of bolted top-and-seat angle connections. *J. Struct. Eng.*, Vol. 129, No.12, p. 1615–1625.

Garlock, M., Ricles, J., and Sause, R. (2005), "Experimental Studies on Full-Scale Post Tensioned Steel Connections", *ASCE J. Struct. Eng.*, **131**(3), 438-448.

Garlock, M., Sause, R. and Ricles, J. (2007), "Behavior and Design of Post-tensioned Steel Frames System", *ASCE J. Struct. Eng.*, **133**(3), 389.

Guo, T., Song, L. and Zhang, G. (2011), "Numerical simulation of the seismic behavior of self-centering steel beam-column connections with bottom flange friction devices", *Eathq. Eng. & Eng. Vib.*, **10**, 229-238. DOI: 10.107/s11803-011-0061-5.

Leon, R.T. and Shin, K.J. (1995), "Performance of Semi-rigid Frames", *Proceedings of Structure Congress*, 1020-1035, April.

López-Barraza, A., Bojórquez, E., Ruiz, S.E. and Reyes-Salazar, A. (2013), "Reduction of Maximum and Residual Drifts on Posttensioned Steel Frames with Semirigid Connections", *Adv. Mater. Sci. Eng.*, Article ID 192484, 11 pages.
DOI: 10.1155/2013/192484.

McCormick, J., Aburano, H., Ikenaga, M. and Nakashima, M. (2008), "Permissible residual deformation levels for building structures considering both safety and human elements", *The 14th Conference on Earthquake Engineering,* Beijing, China, 12-17 October.

Nader, M.N. and Astaneh, A. (1991), "Dynamic behavior of flexible, simirigid and rigid frames", *J. Construct. Steel Res.*, **18**, 179-192.

Reyes-Salazar, A. (2000), "Dissipation of energy in steel frames with PR connections", *Struct. Eng. Mech. Int. J.*, **9**(3), 241-256.

Richard, R.M. and Abbott, B.J. (1975), "Versatile Elastic Plastic Stress-Strain Formula", *ASCE J. Eng. Mech.,* **101**(4), 511-515.

Richard R.M., PRCONN (1993), Moment-rotation curves for partially restrained connections, *RMR Design Group*, Tucson, Arizona.

Ricles, J.M., Sause, R., Garlock, M. and Zhao, C. (2001), "Posttensioned seismic-resistant connections for steel frames"*, ASCE J. Struct. Eng.*, **127**(2), 113-121.

Ricles, J.M., Sause, R., Peng, S.W. and Lu, L.W. (2002), "Experimental evaluation of arthquake resistant post-tensioned steel connections", *ASCE J. Struct. Eng.*, **128**(7), 850-859.

Rojas, P., Ricles, J.M. and Sause, R. (2005), "Seismic Performance of Post-tensioned Steel Moment Resisting Frames with Friction Devices", *ASCE J. Struct. Eng.*, **131**(4),

529-540.

SAC/BD-97/02, "Protocol for Fabrication, Inspection, Testing, and Documentation of Beam-Column Connection Tests and Other Experimental Specimens", by P. Clark, K. Frank, H. Krawinkler and R. Shaw, Appendix E: "Loading Protocol For Stepwise Increasing Cyclic Test".

Shen, J. and Astaneh-Asl, A. (2000), "Hysteretic model of bolted-angle connections", *J. Construct. Steel Res.*, **54**, 317-343.

Shen, J. and Astaneh-Asl, A. (1999), "Hysteretic behavior of bolted angle connections", *J. Construct. Steel Res.*, **51**, 201-218.

Weaver, W. and Gere, J.M. (1980), *Matrix Analysis of Framed Structures*, 2nd Edition, Van Nostran Reinhold Company.

Wolski, M., Ricles, J.M. and Sauce, R. (2009), "Experimental study of a self-centering beam-column connection with bottom flange friction device", *ASCE J. Struct. Eng.*, **135**(5), 479-488.

Yang, J.G and Jeon, S.S. (2009), "Analytical Model for the Initial Stiffness and Plastic Moment Capacity of an Unstiffened Top and Seat Connection under a Shear Load", *Int. J. Steel Struct.*, **9**(3), 195-205.